REPORT DOCUMENTATION PAGE

AFRL-SR-AR-TR-06-0028

1. REPORT DATE *(DD-MM-YYYY)*	2. REPORT TYPE	3. DATES COVERED *(From - To)*
	FINAL REPORT	1 JUN 05 TO 31 OCT 05

4. TITLE AND SUBTITLE
SMART GOLD NANOBOWLS ("NANO-CRESCENT MOON") WITH SUB-10 NM CIRCULAR EDGE FOR LOCAL ELECTROMAGNETIC FIELD ENHANCEMENT EFFECT, SPATIAL, AND NIR TEMPORAL/ THERMAL MODULATIONS FOR MOLECULAR AND CELLULAR DYNAMIC IMAGING

5a. CONTRACT NUMBER
FA9550-05-1-0364

5b. GRANT NUMBER

5c. PROGRAM ELEMENT NUMBER

6. AUTHOR(S)
PROF LUKE P. LEE

5d. PROJECT NUMBER

5e. TASK NUMBER

5f. WORK UNIT NUMBER

7. PERFORMING ORGANIZATION NAME(S) AND ADDRESS(ES)
UNIVERSITY OF CALIFORNIA, BERKELEY
DEPARTMENT OF BIOENGINEERING
485 EVANS HALL #1762, BERKELEY, CA 94720-1762

8. PERFORMING ORGANIZATION REPORT NUMBER

9. SPONSORING/MONITORING AGENCY NAME(S) AND ADDRESS(ES)
AFOSR/NL
875 NORTH RANDOLPH STREET
SUITE 325, ROOM 3112
ARLINGTON, VA 22203-1768

10. SPONSOR/MONITOR'S ACRONYM(S)

11. SPONSOR/MONITOR'S REPORT NUMBER(S)

12. DISTRIBUTION/AVAILABILITY STATEMENT
APPROVED FOR PUBLIC RELEASE, DISTRIBUTION IS UNLIMITED

13. SUPPLEMENTARY NOTES

14. ABSTRACT
Cell signaling involves the production and activation of many intracellular biomolecules. The dynamic detection of the biomolecular reactions is essential to understand the undefined signaling pathway. Current fluorescence based methods have difficulty to detect the dynamic reactions of biomolecules such as nucleolytic, proteolytic, and phosphorylation. In contrast, label-free Raman scattering spectroscopy can detect subtle biochemical changes without fluorescent molecules. First, we have created gold-based nanocrescent Surface Enhanced Raman Scattering 9SERS) probes which can function as the substrate to enhance Raman scattering signal for tens orders of magnitude. Once functionalized with oligonucleotides and peptides, the internalized nanocrescent particles can be used to monitor the enzymes inside the single living cell. In the past ten months, in addition to gold-based nanocrescent SERS probes, we have accomplished the multilayer composite nanocrescent SERS probes with magnetic thin film layer inside of gold nanocresents.

15. SUBJECT TERMS

16. SECURITY CLASSIFICATION OF:			17. LIMITATION OF ABSTRACT	18. NUMBER OF PAGES	19a. NAME OF RESPONSIBLE PERSON
a. REPORT	b. ABSTRACT	c. THIS PAGE			19b. TELEPHONE NUMBER *(Include area code)*

Final Technical report for AFOSR grant FA9550-05-1-0364

Title:

Smart Gold Nanobowls ("Nano-Crescent Moon") with Sub-10 nm Circular Edge for Local Electromagnetic Field Enhancement Effect, Spatial, and NIR Temporal/Thermal Modulations for Molecular and Cellular Dynamic Imaging

P. I. Prof. Luke P. Lee
Lloyd Distinguished Professor
Department of Bioengineering, University of California, Berkeley
Director, Biomolecular Nanotechnology Center
Co-Director, Berkeley Sensor and Actuator Center
485 Evans Hall #1762, Berkeley, CA 94720-1762
Tel: 510-642-5855, Fax: 510-642-5835, Email: lplee@berkeley.edu;
http://biopoems.berkeley.edu

Program Manager, Dr. Hugh DeLong

January 31, 2005

Intracellular Molecular Imaging of Cell Signaling using Nanocrescent SERS Substrates

Summary

Cell signaling involves the production and activation of many intracellular biomolecules. The dynamic detection of the biomolecular reactions is essential to understand the undefined signaling pathway. Current fluorescence based methods have difficulty to detect the dynamic reactions of biomolecules such as nucleolytic, proteolytic, and phosphorylation. In contrast, label-free Raman scattering spectroscopy can detect subtle biochemical changes without fluorescent molecules. First, we have created gold-based nanocrescent Surface Enhanced Raman Scattering (SERS) probes which can function as the substrate to enhance Raman scattering signal for tens orders of magnitude. Once functionalized with oligonucleotides and peptides, the internalized nanocrescent particles can be used to monitor the enzymes inside the single living cell. In the past ten months, in addition to gold-based nanocrescent SERS probes, we have accomplished the multilayer composite nanocrescent SERS probes with magnetic thin film layer inside of gold nanocrescents. The Raman scattering signal can be modulated by the external magnetic field. Second, the nanocrescent particles are modified with PSA substrate peptides and used to detect the prostate specific antigen (PSA), a prominent biomarker for prostate cancer. Last, the nanocrescent particles are modified with p60c-Src peptides and used to detect the activation of tyrosine kinase in single living cells.

PART I. Multilayer Composite Nanocrescent with Magnetic Activity

Surface-enhanced Raman scattering (SERS) spectroscopy shows chemical bond information and it is one of the best methods for label-free biomolecular imaging. Conventional SERS substrates require multiple plasmonic couplings via many colloidal nanoparticles and it is difficult to control the coupling distance. Here, we report the design, fabrication, and

characterizations of a biocompatible composite (Au/Ag/Fe/Au) nanocrescent SERS nanoprobe, which can function not only as a standalone SERS substrate with integrated SERS hot spot geometries, but also has a magnetic controllability in orientation and translation motions. The single nanocrescent demonstrates a SERS enhancement factor higher than 10^8 in the detection of sub-zeptomole molecules. Magnetically modulated SERS detection of molecules on a single composite nanocrescent probe is demonstrated. The gold surfaces of composite nanocrescent SERS probes are biocompatible and can be biofunctionalized and applied in real-time biomolecular imaging.

Unlike conventional fluorescence imaging, Raman spectroscopy acquires unique signatures of chemical and biological molecules without labeling with fluorophore molecules [1]. Raman imaging of living cells can nondestructively probe the intracellular biochemical dynamics without prior fluorescent or radioactive labeling [2], but the formidably low efficiency of Raman scattering hinders its applications in the detection of molecules at micromolar or lower concentrations. However, Surface Enhanced Raman Scattering (SERS) by metallic nanostructures increases the original Raman scattering intensity for many orders of magnitude, which makes the Raman detection of low concentration molecules practical [3]. Colloidal Au or Ag nanoparticle clusters are commonly used as SERS substrates, and Raman enhancement factors as high as 10^{14} have been reported in single molecular level detections [4, 5]. Au and Ag nanoparticles are also utilized in Raman cellular imaging to enhance signal intensity and increase image contrast [6]. However conventional nanoparticles have inherent limits for *in vivo* biomolecular SERS imaging in that 1) strong Raman enhancement relies on good coupling between adjacent nanoparticles, so called "hot spot", which is inconsistent for randomly formed nanoparticle clusters, 2) the spatial imaging resolution degrades with increasing size of nanoparticles clusters, 3) the random distribution of nanoparticles within the biological cell voids the spatial specificity. We have previously developed Au nanocrescent structures with sub-10nm sharp edges that can be used as excellent standalone SERS probes [7]. In comparison with other available single-

nanoparticle-based SERS substrates such as nanoshell [8], nanotip [9], and nanoring [10], the Au nanocrescent has a higher local field enhancement factor in the near infrared wavelength region due to the simultaneous incorporation of SERS hot spots including sharp nanotip and nanoring geometries and thus the strong hybrid resonance modes from nanocavity resonance mode and tip-tip intercoupling mode. However, the previously demonstrated Au nanocrescent is inconvenient in practical applications and especially intracellular SERS sensing because the orientation and position of the gold nanocrescent are random. In fact controllable micro- or nanoparticles have been extensively used in biomolecular and cellular sensing by means of magnetic, electric or optical control schemes. Magnetically modulated fluorescent microparticles were demonstrated to achieve higher signal-to-noise ratio in fluorescence imaging [11].

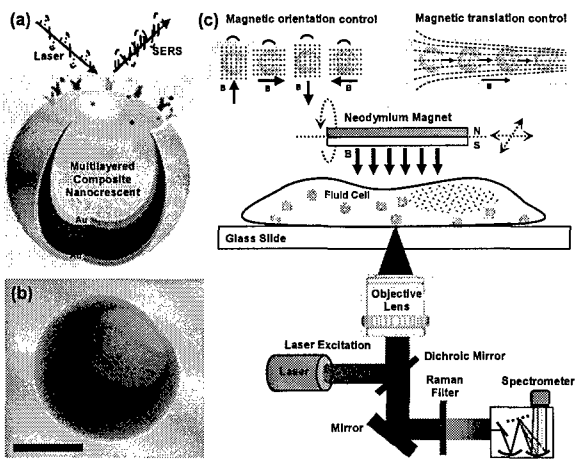

Fig. 1. Composite-material magnetic nanocrescent SERS probes. **(a)** Schematic diagram of SERS detection on a single composite nanocrescent. **(b)** TEM image of a single magnetic nanocrescent SERS probe. The scale bar stands for 100 nm. **(c)** Schematic diagram of SERS imaging system and the magnetic manipulation system for intracellular (in fluids) biomolecular imaging using standalone magnetic nanocrescent SERS probes.

Here we report magnetically controllable nanocrescent SERS probes by incorporating composite layers with ferromagnetic material (Fig. 1a). Nanostructured composite multilayer design (Au/Ag/Fe/Au) with magnetic thin film allows an ideal biophotonic molecular probe controllable with external magnetic field. The fabrication process of a composite nanocrescent (see

supplemental Fig. S1) is similar to the fabrication process reported previously [7] while forming a multilayer of 10 nm Au, 10 nm Fe, 20 nm Ag and 10 nm Au. The detail on fabrication is described in the experimental section. The choice of materials and multilayer thickness are intentionally designed with the assistance of finite element simulation in order to tune the plasmon resonance wavelength of the composite nanocrescent matched with the excitation wavelength. The nanocrescent has a sub-10 nm sharp edge, although the multilayer structure is not clearly distinguishable in the TEM image (Fig. 1b) due to the low imaging contrast between the different metallic materials of Au, Ag, or Fe. The nanocrescents suspended in the fluids are then controlled by magnetic fields during the SERS imaging process (Fig. 1c).

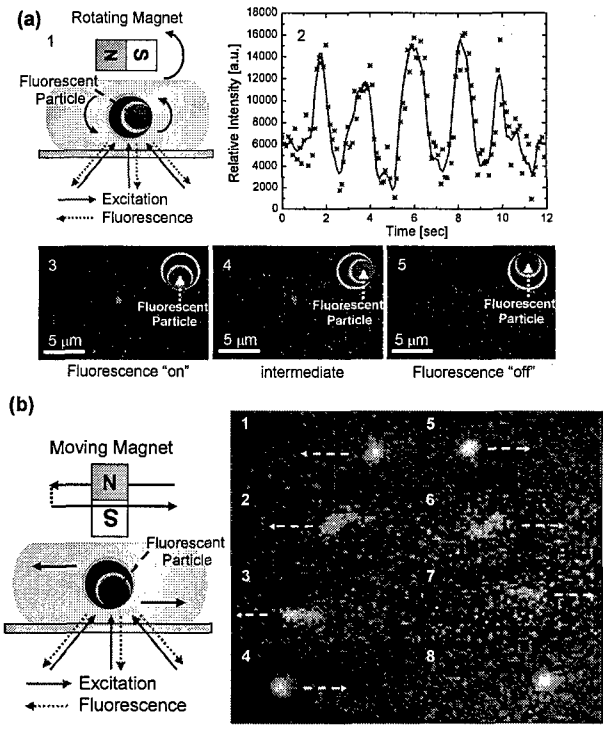

Fig. 2. Magnetic manipulation of a single nanocrescent attached to a fluorescent polystyrene nanosphere. **(a)** Magnetically modulated rotation of a single nanocrescent. 1) Schematic diagram of the experimental setup. The orientation of the nanocrescent follows the rotation of the permanent magnet at the frequency of 0.5 Hz; 2) modulated fluorescence intensity of the nanocrescent as the function of time; 3), 4), and 5) show the representative images of the nanocrescent with different orientations when the fluorescence intensity is maximal 3), minimal 5) and in between 4). **(b)** Schematic diagram and the fluorescence images of the magnetically modulated lateral translation of a single fluorescent nanocrescent. The frame 1 to frame 8 are

representative images taken with 0.5 second time-interval showing the single fluorescent nanosphere is moved back and forth horizontally by moving the magnet.

In addition to magnetostatic force, the reduced symmetry geometrical shape of the nanocrescent enables net torque to be generated by an external magnetic field (supplemental Fig. S2). Hence the nanocrescent can be both moved and oriented by controlling the external magnetic field. To observe the responses of nanocrescents to magnetic modulation, some nanocrescents are intentionally fabricated using fluorescent polystyrene nanosphere templates (150 nm in diameter). In this case we used the fluorescent polystyrene nanosphere template without removing it, which enables the use of an epi-fluorescence video microscopy system in tracking the movements of the nanocrescents at high speeds during the magnetic manipulation. A neodymium permanent magnet is mounted in a close proximity above a closed microfluidic cell with nanocrescents suspended in liquid. By rotating the permanent magnet at the frequency of 0.5 Hz and varying the orientation of the magnetic field, the orientation and fluorescence intensity of the fluorescent nanocrescents can be modulated as shown in Fig. 2a. The fluorescence intensity is higher when the excitation light directly impinges on the fluorescent nanosphere, while the fluorescence intensity is lower when the metallic multilayer blocks the excitation light path. Due to the thermal tumbling of the nanocrescent and slight change of magnetic field component in the lateral direction, jitters in the modulated fluorescent signal can be observed, but the position of the nanocrescent remains within a ~3μm×3μm square block during the rotation process. Fig. 2b shows the lateral translation of a single fluorescent nanocrescent controlled by the permanent magnet. The sequential image frames is taken every half second during the lateral movement of the nanocrescent. The lateral motions of the nanocrescents are limited to certain image plane (variation within vertical resolution of the 40X objective lens, ~10 μm) due to the balances between gravity, buoyancy, drag and magnetic force in the vertical direction, although the magnetic field component in the vertical direction slightly changes during the lateral motion of the permanent

magnet. We found the vertical motion of nanocrescents is much more insensitive to magnetic actuations than lateral motion.

In contrast to spherical metallic nanoparticles, the nanocrescent has plasmon resonance modes in the near infrared light region and a much higher local field enhancement (~20 dB of electric field amplitude). However, the enhancement factor and local field distribution are dependent on the orientation of nanocrescent with respect to the incident direction of excitation light as shown in the finite element simulation (Fig. 3a). We used FEMLAB electromagnetic simulation software (COMSOL, CA) to generate the results. The maximum local field enhancement is achieved when the propagation direction of the excitation field is parallel to the symmetry line of the nanocrescents. In an experiment, a circularly polarized near infrared laser (785 nm) is focused on the nanoparticles by a high numerical aperture microscopy objective lens. No optical filter is used in this measurement. The local field intensity measured from far field shows that the enhancement by a single nanocrescent shown in the right image of Fig. 3b is larger than 5 folds, which cannot be attributed to reflections from the metallic surface because reflection becomes negligible and scattering dominates for structures much smaller than the excitation wavelength. In contrast, another nanocrescent shown in the middle image of Fig. 3b only generates 2~3 folds of enhancement possibly due to a different orientation, which verifies that the local field enhancement of the composite nanocrescents depends on their orientations. The inset drawings in Fig. 3b illustrate the possible orientations of the mentioned two nanocrescents, and the cross-line intensity plots further clarify the orientation-dependent field enhancement effect. 80 nm Au nanospheres are also tested but no significant field enhancement effect is observed at the 785 nm excitation wavelength.

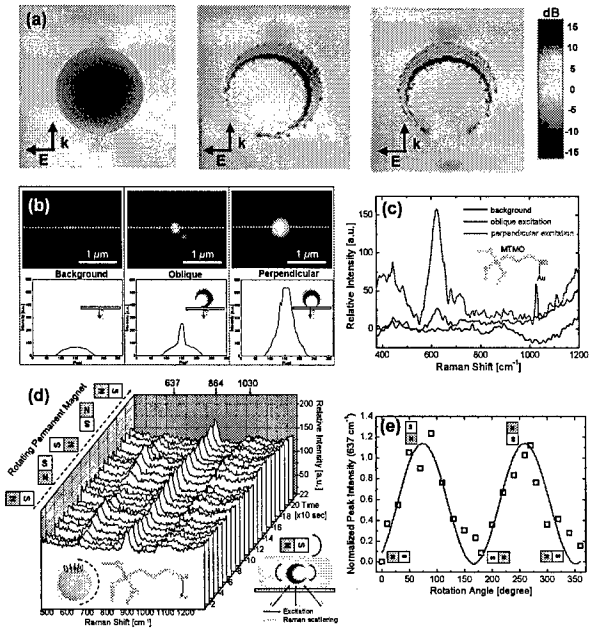

Fig. 3. Magnetically modulated SERS detection of MTMO molecules tethered on a single nanocrescent. **(a)** Simulated local electric field amplitude enhancement in the unit of dB by a single nanocrescent with 0° (right) and 45° (middle) respect to the 785 nm light incident direction in comparison with an 80 nm Au nanosphere (left). **(b)** Intensity images and the cross-line intensity plots of laser focal spot without nanocrescent (left), with a single nanocrescent obliquely (middle) and perpendicularly (right) oriented with respect to the direction of excitation laser light. **(c)** SERS spectra of MTMO molecules on the surface of the glass slide (background), and on the single nanocrescents with oblique and perpendicular orientations. **(d)** Series of SERS spectra as the function of time when continuously changing the external magnetic field direction. **(e)** Intensity plot of the 637 cm^{-1} Raman peak vs. approximate rotational angles of the permanent magnet.

We also compare the SERS spectra of chemical molecules immobilized on the surfaces of the above two nanocrescents. A self-assembly-monolayer of 3-mercaptopropyltrimethoxy-silane (MTMO), a thiol-group containing molecule, is attached to the surface of the nanocrescents through Au-sulfide bonds by spreading and drying a droplet of 1 μM MTMO in anhydrous ethanol solution. Fig. 3c shows the SERS spectra of MTMO molecules on the background substrate and the nanocrescents in two different orientations. The spectra are taken using a laser excitation with 1mW power and integration time of 20 seconds. In accordance with the trend shown in the far-field scattering intensity measurement, the SERS enhancement factor of the perpendicularly-oriented nanocrescent is

higher than that of the obliquely-oriented nanocrescent by comparing the intensity of 637 cm^{-1} Raman peak.

Since the orientation of suspended nanocrescents can be controlled dynamically by an external magnetic field, the SERS signal of MTMO molecules immobilized on the surface of a single nanocrescent can also be modulated magnetically. We prepared the 1μM-MTMO-tethered nanocrescents suspended in 1M ethanol solutions. The same magnet setup is used to apply the magnetic field. After the nanocrescents are stabilized under a constant magnetic field, the SERS spectra from a single nanocrescent are continuously taken while the orientation of the external magnetic field is changing. The integration time of spectra acquisition is 10 seconds, and every spectrum is taken after the magnet rotates for approximately 20 degrees and the laser spot is tightly focused on the particle. Fig. 3d shows the series of SERS spectra as the function of time. The intensity of 637 cm^{-1} Raman peak from MTMO molecules varies periodically and responds to the rotation of the permanent magnet. On the contrary, the intensity of the 864 and 1030 cm^{-1} peaks from the internal control, 1M ethanol, remains relatively stable. It has been reported that solvent molecules such as methanol and ethanol in water will not be adsorbed on the substrate surface and not undergo the SERS effect [12]; therefore the intensity of the Raman peaks from the solvent molecule can serve as an internal reference to calculate the Raman enhancement factor. Fig. 3e shows the intensity of 637 cm^{-1} peak vs. the rotational angle of the permanent magnet. The shown peak intensities are normalized to control peak intensities at 864 cm^{-1} for the correction of laser intensity fluctuations. The maximal SERS enhancement factor from the single nanocrescent at the perpendicular orientations is above 10^6 (1 M : 1 μM) with respect to the internal control, and ~7 times higher than that of the minimal enhancement from the nanocrescent at the oblique orientations. In fact, the enhancement factor could be even larger if only comparing the number of target molecules adsorbed on the nanocrescent with that of the solvent molecules present in the laser spot focal volume. The detectable volume of the solvent molecules is ~100 times larger than that of the adsorbed target molecules [13].

Therefore the actual number of the target molecules can be 10^8 times smaller than that of the solvent molecules within the detectable focal volume, which results a Raman enhancement factor higher than 8 orders of magnitudes and the detection of less than zeptomole molecules. Since the Raman peak intensities of the solvent molecules, equivalent to a DC signal, are constant, the signal to noise ratio of the SERS detection (AC signal) can be improved through magnetic modulation, which is especially important when the Raman peaks from a complex background are as high as those of the tethered target molecules.

We demonstrated the multilayer composite nanocrescent SERS probes in one particular size for the clarity and consistency throughout. In fact, the size, shape and layer thickness can all be individually controlled by modifying the size of the sacrificial nanosphere template, the deposition angle, the deposited layer thickness and the material of each layer. Since the plasmon resonance wavelength of the metallic nanostructures is dependent on these parameters, the optical properties of the nanocrescent are tunable in our fabrication process. More studies on the optical properties of nanocrescents are underway. The Raman enhancement factor of single nanocrescent is as high as those reported for nanoparticle clusters and it is suitable for high-resolution biomolecular sensing in living cells. Furthermore, it can be precisely manipulated with proper magnetic field control. The biocompatible Au surface can also be functionalized by tethering oligonucleotide, peptide or antibodies using well established methods [14]. The nanocrescent responds to near infrared excitation which has deeper penetration and results in less photo-thermal damage to cell tissue. Owing to the above reasons, the biochemical composition of the local intracellular environment at nanometer scale can be potentially measured by the translocation of standalone magnetic nanocrescent SERS probes to a desired position within living cells and detecting the fingerprints of biomolecules dynamically. The orientation modulation of nanocrescents by magnetic field can further increase the signal to noise ratio in the dynamic SERS detections.

Reference

[1] C. V. Raman, *Nature* **1928**, *121*, 619.

[2] Y. S. Huang, T. Karashima, M. Yamamoto, T. Ogura, H. Hamaguchi, *J. of Raman Spectrosc.* **2004**, *35*, 525.

[3] Fleischm.M, P. J. Hendra, Mcquilla.Aj, *Chem. Phys. Lett.* **1974**, *26*, 163.

[4] S. M. Nie, S. R. Emery, *Science* **1997**, *275*, 1102.

[5] K. Kneipp, Y. Wang, H. Kneipp, L. T. Perelman, I. Itzkan, R. Dasari, M. S. Feld, *Phys. Rev. Lett.* **1997**, *78*, 1667.

[6] K. Kneipp, A. S. Haka, H. Kneipp, K. Badizadegan, N. Yoshizawa, C. Boone, K. E. Shafer-Peltier, J. T. Motz, R. R. Dasari, M. S. Feld, *Appl. Spectrosc.* **2002**, *56*, 150.

[7] Y. Lu, G. L. Liu, J. Kim, Y. X. Mejia, L. P. Lee, *Nano Lett.* **2005**, *5*, 119.

[8] S. J. Oldenburg, S. L. Westcott, R. D. Averitt, N. J. Halas, *J. of Chem. Phys.* **1999**, *111*, 4729.

[9] A. Hartschuh, E. J. Sanchez, X. S. Xie, L. Novotny, *Phys. Rev. Lett.* **2003**, *90*, 095503.

[10] J. Aizpurua, P. Hanarp, D. S. Sutherland, M. Kall, G. W. Bryant, F. J. G. de Abajo, *Phys. Rev. Lett.* **2003**, *90*, 057401.

[11] J. N. Anker, R. Kopelman, *Appl. Phys. Lett.* **2003**, *82*, 1102.

[12] K. Kneipp, H. Kneipp, R. Manoharan, E. B. Hanlon, I. Itzkan, R. R. Dasari, M. S. Feld, *Appl. Spectrosc.* **1998**, *52*, 1493.

[13] The focal volume can be approximated as the volume of the cylindrical beam waist whose radius r = 0.5 μm, length h = 5 μm, that is, $\pi \times r^2 \times h = \pi \times (0.5)^2 \times 5\ \mu m^3 \approx 3.8\ \mu m^3$, while the volume of the single nanocrescent is about $\pi \times 4/3 \times (0.2)^3\ \mu m^3 \approx 0.038\ \mu m^3$.

[14] Y. W. C. Cao, R. C. Jin, C. A. Mirkin, *Science* **2002**, *297*,153 6.

PART II SERS Detection of Prostate Specific Antigen

Prostate cancer incidence and mortality rates vary worldwide. It is the most common cancer in men in Europe and North America [1-3]. In the United States, prostate cancer is the second-leading cause of cancer death for men. One of the clinical diagnosis tools for prostate cancer is the measurement of plasma protein concentration of the prostate-specific antigen (PSA or hK3). PSA is a member of the large kallikrein (hK) protease family (for reviews, see[4-6]), which is normally secreted from prostate luminal epithelial cells. Unlike other kallikrein family members, PSA is a chymotrypsin-like serine protease[7]. Upon ejaculation, PSA rapidly hydrolyzes both semenogelin I and semenogelin II *in vivo*, as well as fibronectin, resulting in the liquefaction of the semem coagulum, where spermatozoa are originally trapped. PSA activity is important in initiating the spermatozoa forward motility. In prostate cancer, PSA, and perhaps, other members of the hK family proteases, are involved in tissue remodeling aided by the proteolytic activities against the extracellular matrix, contributing critical control mechanisms to tumor invasion or progression.

The introduction of plasma PSA screening since the 1980s has greatly improved the diagnosis, staging, and management of prostate cancer[5]; however, many problems exist with this method. Measurement of plasma PSA concentration does not differentiate the prostate cancer patients from those with benign prostatic hyperplasia, leading to a high false positive rate, requirement for more expensive biopsies, and even unnecessary surgical procedures[5, 6]. Efforts to enhance the clinical value of the PSA for early detection of prostate cancer have included the characterization of various molecular variants of PSA, since PSA in prostate cancer exists in various isoforms and proteolytic activity [8-10]. Among those various isoforms, the proteolytically active subpopulation of PSA is a more useful tumor marker than the serum PSA concentration and is a better predictor for prostate cancer malignancy[11, 12]. Simple detection of the presence of PSA by a traditional immunostaining method can not reveal the proteolytic activity of the PSA; therefore, it is of great importance to develop new methods to

discriminate the different PSA isoforms, especially the proteolytically active form. Seminal fluid has been demonstrated to carry an abundance of proteolytically active PSA and is a biological source of PSA for protease activity assays [13, 14]. The concentration of proteolytically active PSA in seminal fluid can very high, 10-150 M[14], while its concentration in the plasma is much lower, from less than 0.1nM in healthy individuals to higher than 1nM in patients with prostate disease[15]. However, an assay that measures the proteolytic activity of PSA in seminal fluid is still not widely accepted, due to the quick decay of the proteolytic activity, the limited amount of seminal fluid available from old patients, and the difficulty in obtaining accurate results.

So far, various modalities have been used in PSA detection including ELISA [16], gel electrophoresis [17], antibody fluorescence labeling [18], etc. The sensitivity of current detection methods is limited to nanomolar concentrations, and relatively large sample volume (milliliter) is required. Here we introduce a new optical spectroscopic detection method for PSA proteolytic activity based on a peptide-conjugated crescent nanoparticle, which can be used on minute sample volumes (femtoliters), integrated into microfluidics, and multiplexed as high density nanoarrays or microarrays (with sub-microliter volume). The nanocrescent can serve as an individual surface enhanced Raman scattering (SERS) substrate [19], and after conjugation with a peptide specifically designed for PSA[7, 12-14, 20], it can be used to optically monitor PSA proteolytic reactions. Raman is a sensitive spectroscopic detection method for probing biochemical composition with abundant atomic level information without fluorophore labeling[21], however the Raman signal intensity (scattering cross-section) is much lower than fluorescence. Various SERS substrates have been developed to enhance the weak Raman scattering signals in chemical and biomolecule detections on the substrate surface over several orders of magnitude [19, 22-27]. The nanoscale dimension and the high local electromagnetic field enhancement of our nanocrescent SERS substrate enable a high-sensitivity optical detection of biomolecular reactions on its surface (Figure 1c).

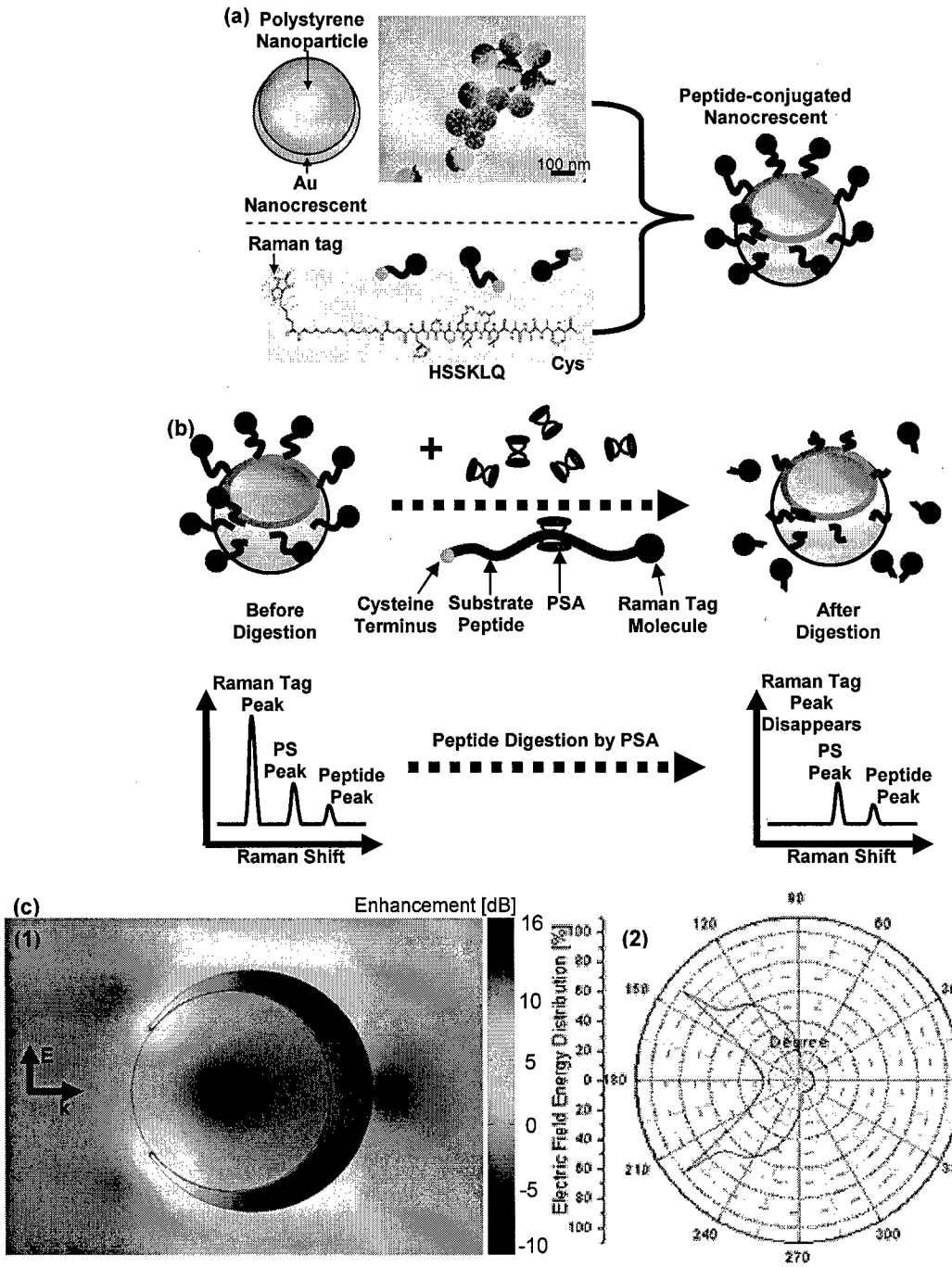

Fig. 1 Peptide-conjugated nanocrescent for PSA detection. **(a)** Fabrication procedure. The nanoscale Au layer is evaporated on polystyrene nanoparticles to form the Au nanocrescent as shown in the TEM image, with the crescent tip showing lighter density. Peptides are synthesized with the specific PSA substrate sequence HSSKLQ and are terminated by a Raman tag molecule, biotin or R19 (not shown), respectively, and cysteine for both versions of tagged peptides. The

peptides are conjugated to the Au surface of the nanocrescents through an Au-S bond. **(b)** PSA detection scheme. Before the proteolytic reaction, the SERS spectrum of the peptide-conjugated nanocrescent contains the characteristic peaks from the Raman tag molecules, polystyrene nanoparticle, and the peptides; after the digestion reaction by PSA, the peptide is cleaved between L and Q. The cleavage fragment containing the Raman tag molecules diffuses away from the nanocrescent surface, while the other fragment remains on the nanocrescent surface. The SERS spectrum of the peptide becomes different and the characteristic peaks from the Raman tag molecule disappear. **(c)** (1) Simulated local electric field amplitude enhancement by nanocrescent. The tip region of the nanocrescent has an electromagnetic enhancement factor of 100 fold. (2) Polar electric field energy distribution on the nanocrescent. Almost 100% energy is concentrated near the tip area which accounts for ~1/6 of total area of the nanocrescent.

The nanocrescents consist of a 100 nm polystyrene core and a 10~20 nm gold crescent shell. Fig. 1a shows the schematics and transmission electron micrograph of the nanocrescent. The nanocrescents are fabricated by angled Au deposition on the rotating polystyrene nanoparticle template[19]. The fabrication details were described previously[19]. The polystyrene nanoparticle core is not removed and it serves as the internal control in the SERS detections. We then tether a specially designed peptide on the surface of the Au nanocrescent. The peptides contain the sequence of HSSKLQ which has been shown to have very high specificity to PSA [28]. A cysteine group at the carboxyl terminus of the peptide is used to attach the peptide to the Au surface, relying on the Au-thiol reaction to form a covalent bond. At the amino terminus of the peptide, Raman active molecules such as biotin (shown in figure 1a) or Rhodamine 6G (R19) (not shown in the schematics) are grafted through a short polyethyleneglycol or aminovaleric acid linker. The detection scheme is shown in Fig. 1b. The SERS spectra of the artificial peptides change after digestion by PSA, and the characteristic SERS peaks of the molecular moieties with the biotin or R19 tags disappear due to the diffusive dislocation of the tag molecules from the nanocrescent surface into the solution after peptide digestion; therefore the existence and concentration of the proteolytically PSA in solution can be probed by monitoring the SERS spectra of the peptide-conjugated nanocrescents. The Raman scattering signal of the peptide change is amplified by the nanocrescent.

Our numerical simulation (Fig. 1c) indicates the amplitude of the local electric field can be enhanced by close to 20 dB (100 fold) especially around the sharp edge. Due to the fourth power relation between the electric field amplitude and the Raman enhancement factor, the peptide Raman signal could be amplified 10^8 times by the nanocrescent.

Fig. 2 shows the experimental system configuration. The peptide-conjugated nanocrescents are incubated with PSA molecules in a closed transparent microchamber to minimize evaporation. The transparent microchamber is mounted on a 37 °C thermal plate on an inverted Raman microscope with darkfield illumination for nanoparticle visualization. The inset pictures show the ~0.8 mW excitation laser spot focusing on a single nanocrescent.

The typical SERS spectra of the peptide-conjugated nanocrescents with biotin and R19 Raman tag molecules are shown in fig. 3a and 3b, respectively. By comparing the SERS spectra before and 2 hours after the peptide digestion experiments, the Raman peaks from polystyrene core, e.g. 1003 cm^{-1}, remains constant, which serves as an internal control "signal as the indication of stably focused laser excitation" (not sure what quoted phrase is supposed to mean). Some Raman peaks are from the partial amino acid chain remaining on the nanocrescent surface after digestion and they still appear in the spectra, although the peak positions have slight changes and the peak intensities decrease due to possible conformational changes upon peptide cleavage. Those peaks from the Raman tag molecules, such as 525 cm^{-1} from biotin in fig. 3a and 1183 cm^{-1} from R19 in fig. 3b, almost completely disappear after the digestion reaction is finished.

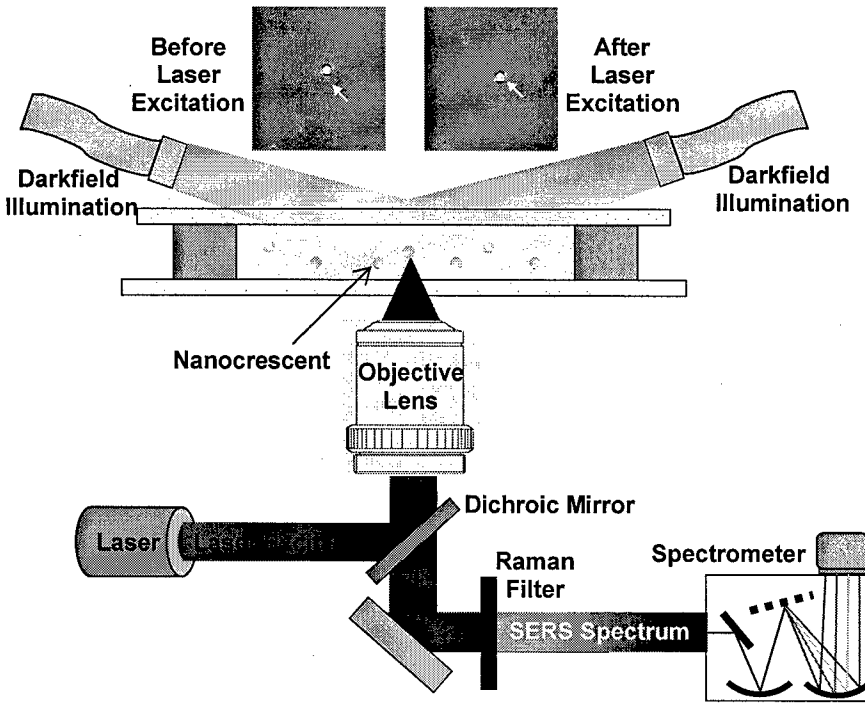

Fig. 2 SERS microspectroscopy system and nanocrescent visualization. The peptide-conjugated nanocrescents are suspended in the reaction buffer in an enclosed transparent microchamber. The nanocrescents can be visualized using the darkfield illumination from oblique angles as the bright dots shown in the inset pictures. The excitation laser is focused on the nanocrescents by a microscopy objective lens. The SERS signal is collected by the same objective lens and analyzed by a spectrometer.

The digestion reaction dynamics can be monitored by time-resolved SERS spectra acquisitions. Because ~100 peptides are conjugated on each nanocrescent on average, the disappearance of the characteristic Raman peaks from the tag molecules is not abrupt. Since most of enhanced field concentrated around the tip area which accounts for ~1/6 of total area of the nanocrescent, the actual molecule number contributing to the Raman scattering signal is less than 20. As shown in the time-lapse SERS spectra in Fig. 3a, the digestion of all of the peptides on each nanocrescent, as monitored by the disappearance of the biotin peak at 525 cm^{-1}, takes ~30 min at a PSA concentration of 420 nM. For

the peptide with R19 as the Raman tag molecule, the disappearance of the R19 peak at 1183 cm^{-1} can be also observed after digestion by 420 nM PSA (Fig. 3b).

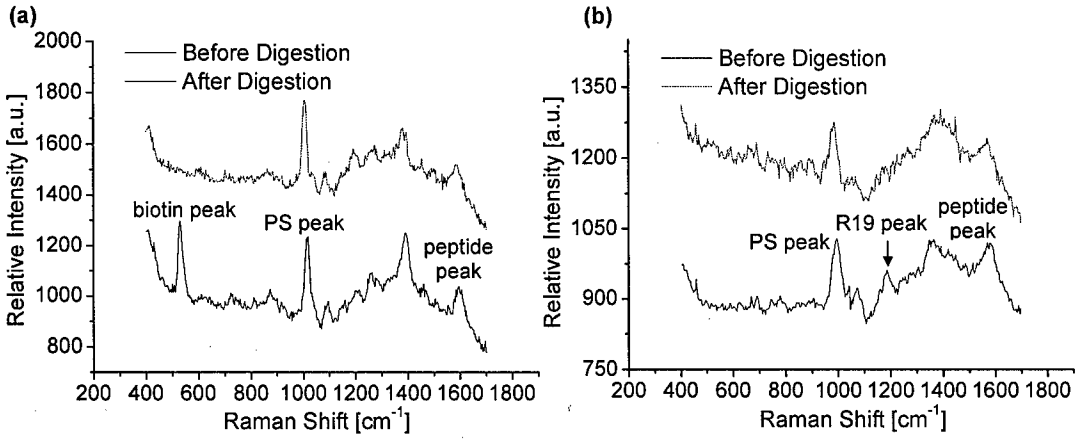

Fig. 3 Typical SERS spectra of peptide-conjugated nanocrescents before and after PSA digestion reactions with **(a)** biotin and **(b)** R19 as the Raman tag molecules respectively.

In order to specifically inhibit the PSA-mediated proteolysis of the conjugated peptides, PSA inhibitors were introduced prior to the addition of 420 nM PSA. We also tested the specificity of the conjugated peptides to PSA using other serine proteases such as Granzyme B, which serves as a negative control here. Fig. 4c and 4d show the time-lapse SERS spectra of nanocrescents with R19 tag molecules in the above two control experiments with the PSA inhibitor and the serine protease Granzyme B, which has orthogonal substrate specificity to PSA, respectively. The peptide digestion by PSA is more than 90% suppressed after the addition of inhibitors given the same experimental conditions. In the control experiment of peptide digestion by 420 nM Granzyme B, the reaction rate showed no statistically significant difference from the inhibitor-treated reaction.

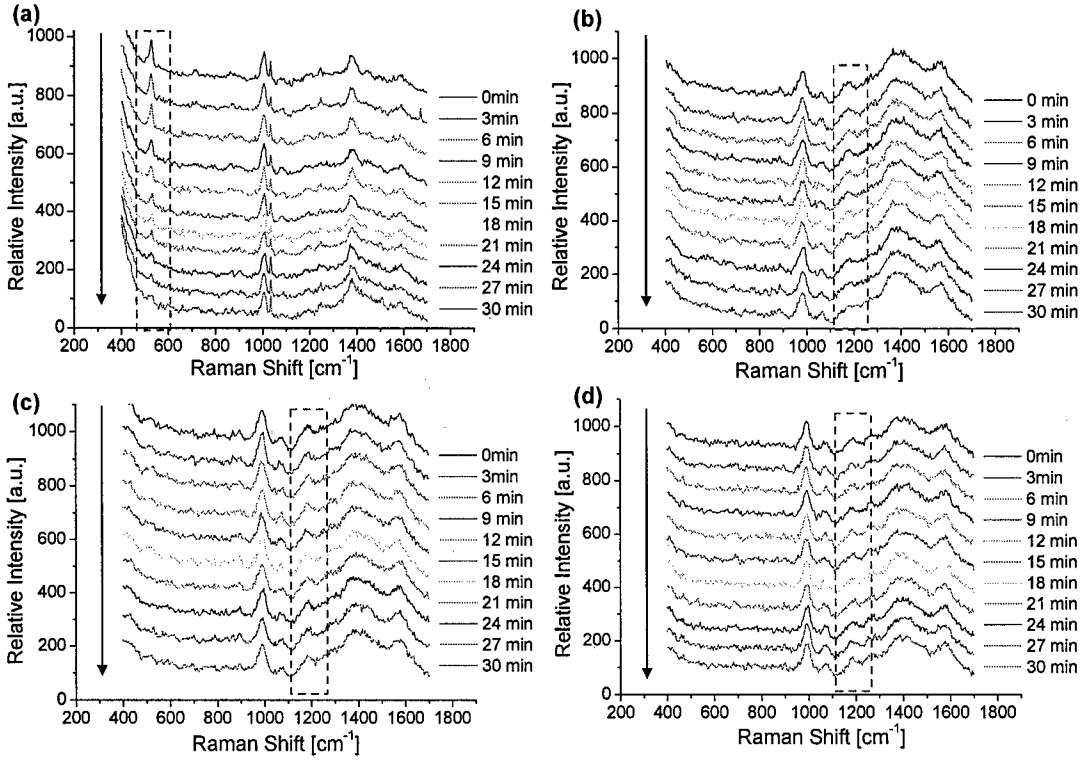

Fig. 4 Time-resolved SERS spectra in PSA digestion reactions. **(a)** SERS spectra in the peptide digestion by 420 nM PSA with biotin as the Raman tag molecule. **(b)** SERS spectra in the peptide digestion by 420 nM PSA with R19 as the Raman tag molecule. **(c)** SERS spectra in the peptide digestion by 420 nM PSA in the presence of inhibitor with R19 as the Raman tag molecule. **(d)** SERS spectra in the peptide digestion by 420 nM Granzyme B with R19 as the Raman tag molecule.

The digestion rate is related to the PSA concentration and we found the minimal PSA concentration detectable in 30 min is around 1 nanomolar (with ~50% reduction in biotin signal intensity, data not shown). Since at most 100 peptide molecules are attached per nanocrescent, it is likely that the nanocrescent surface with the highest SERS signal is not fully taken advantage of, and only a small percentage of the peptides are attached to the region that provides the greatest enhancement in electromagnetic field. Fig. 5a shows the intensities of the biotin Raman peak at 525 cm^{-1} as a function of PSA digestion time for the PSA concentration of 0 M (buffer solution), 4.2 nM, 42 nM and 420 nM. Fig. 5b shows the time-lapse intensities of the R19 Raman peak at 1183 cm^{-}

^{1} in the digestion reaction with 420 nM PSA, 420 nM PSA with inhibitor, and 420 nM Granzyme B, respectively. All the peak intensity values are normalized to the internal control peak at 1003 cm^{-1} and the initial peak intensity at 525 or 1183 cm^{-1}. The results indicate that the peptides are efficiently and specifically cleaved by PSA even after the conjugation with Au nanocrescents; therefore this peptide-conjugated nanocrescent can be used as a specific screening tool to provide information on the concentration and activity of the cancer biomarker PSA.

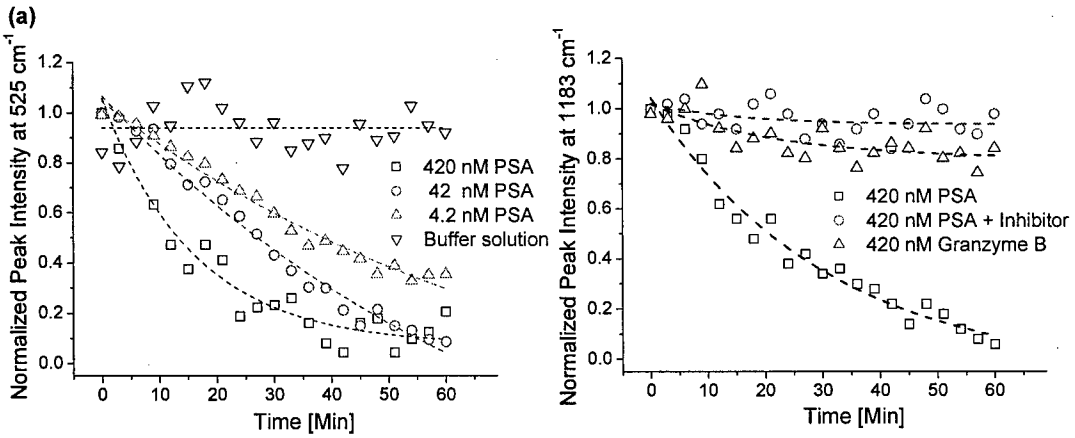

Fig. 5 Time-dependent Raman peak intensities in PSA digestion reactions. **(a)** Raman peak intensities of biotin at 525 cm-1 in the digestion reactions with 0 M (buffer solution), 4.2 nM, 42 nM and 420 nM PSA, respectively. **(b)** Raman peak intensities of R19 at 1183 cm^{-1} in the digestion reactions with 420 nM PSA, 420 nM PSA with inhibitor, and 420 nM Granzyme B, respectively.

In conclusion, we have demonstrated the *in vitro* PSA detection using single peptide-conjugate nanocrescent SERS probes with nanomolar sensitivity. Since we use highly focused laser beam as our excitation source, the detection volume is only about 10 femtolitter. The actual PSA molecule number for the nanomolar samples is close to single molecular level. Compared to other cancer biomarker detection assays, our bioconjugated nanocrescent allows the detection of nanomolar concentrations of proteolytically active PSA molecules in femtoliter volumes, which is crucial especially for cancer screening at a single cancer cell level. The small volume requirement and sensitivity level makes it

possible to detect PSA activity in captured circulating prostate cancer cells for indications of metastasis, which is not feasible with conventional techniques. In semen, the PSA concentration is 10-150 μM, with approximately two thirds of the PSA enzymatically active[20]. The sensitivity level achieved with the nanocrescent PSA probe (nanomolar range) is sufficient for a seminal fluid based assay, thus the nanocrescent SERS platform here could have potential clinical applications. In the current generation design, the PSA digestion site is between the Leucine (L) and Glutamine (Q) residues, and is very close to the Au surface, thus the PSA peptide could be sterically hindered from the PSA enzyme and not optimally accessible. We envision that, with additional spacer synthesized in between the substrate peptide sequence HSSKLQ and the Cys residue, we can improve the presentation of PSA substrate peptide HSSKLQ on the surface, and increase the detection sensitivity consequently. The real-time reaction monitoring also provides abundant information on the PSA activities, not only the presence of the protein. Two different Raman tag molecules are successfully utilized here indicating the potential of multiplexing the peptide-conjugated nanocrescents to detect two or more types of cancer-related proteases. Additional spatial multiplexing in a microarray or nanoarray format is under investigation in our laboratories. In addition, the fabrication scheme of the nanocrescent permits the creation of magnetically or laser maneuverable SERS nanoprobes for biosensing at desired locations[29], which would be useful for obtaining *in situ* measurements intracellularly.

References

1. E.D. Crawford, "Epidemiology of prostate cancer," *Urology* **62**, 3-12 (2003).
2. H. Gronberg, "Prostate cancer epidemiology," *Lancet* **361**, 859-864 (2003).
3. K. J. Pienta, J. A. Goodson, and P. S. Esper, "Epidemiology of prostate cancer: molecular and environmental clues," *Urology* **48**, 676-683 (1996).
4. G. M. Yousef and E. P. Diamandis, "The new human tissue kallikrein gene family: structure, function, and association to disease," *Endocr Rev* **22**, 184-204 (2001).
5. S. R. Denmeade and J. T. Isaacs, "A history of prostate cancer treatment," *Nat Rev Cancer* **2**, 389-396 (2002).

6. S. R. Denmeade and J. T. Isaacs, "The role of prostate-specific antigen in the clinical evaluation of prostatic disease," *BJU Int* **93** Suppl 1, 10-15 (2004).
7. M. Robert, B. F. Gibbs, E. Jacobson, and C. Gagnon, "Characterization of prostate-specific antigen proteolytic activity on its major physiological substrate, the sperm motility inhibitor precursor/semenogelin I," *Biochemistry* **36**, 3811-3819 (1997).
8. S. D. Mikolajczyk *et al*, "Proenzyme forms of prostate-specific antigen in serum improve the detection of prostate cancer," *Clin Chem* **50**, 1017-1025 (2004).
9. S. D. Mikolajczyk, and H. G. Rittenhouse, "Pro PSA: a more cancer specific form of prostate specific antigen for the early detection of prostate cancer," *Keio J Med* **52**, 86-91 (2003).
10. S. D. Mikolajczyk, Y. Song, J. R.Wong, R. S. Matson, and H. G. Rittenhouse, "Are multiple markers the future of prostate cancer diagnostics?" *Clin Biochem* **37**, 519-528 (2004).
11. P. Wu, U. H. Stenman, M. Pakkala, A. Narvanen, and J. Leinonen, "Separation of enzymatically active and inactive prostate-specific antigen (PSA) by peptide affinity chromatography," *Prostate* **58**, 345-353 (2004).
12. P. Wu, L. Zhu, U. H. Stenman, and J. Leinonen, "Immunopeptidometric assay for enzymatically active prostate-specific antigen," *Clin Chem* **50**, 125-129 (2004).
13. M. Brillard-Bourdet et al, "Amidolytic activity of prostatic acid phosphatase on human semenogelins and semenogelin-derived synthetic substrates," *Eur J Biochem* **269**, 390-395 (2002).
14. S. Rehault et al, "Design of new and sensitive fluorogenic substrates for human kallikrein hK3 (prostate-specific antigen) derived from semenogelin sequences," *Biochim Biophys Acta* **1596**, 55-62 (2002).
15. H. G. Rittenhouse, J. A. Finlay, S. D. Mikolajczyk, and A.W. Partin, "Human Kallikrein 2 (hK2) and prostate-specific antigen (PSA): two closely related, but distinct, kallikreins in the prostate," *Crit Rev Clin Lab Sci* **35**, 275-368 (1998).
16. B. Acevedo et al, "Development and validation of a quantitative ELISA for the measurement of PSA concentration," *Clin Chim Acta* **317**, 55-63 (2002).
17. J. P. Charrier, C. Tournel, S. Michel, P. Dalbon, and M. Jolivet, "Two-dimensional electrophoresis of prostate-specific antigen in sera of men with prostate cancer or benign prostate hyperplasia," *Electrophoresis* **20**, 1075-1081 (1999).
18. A. Bjartell et al, "Time-resolved fluorescence imaging (TRFI) far direct immunofluorescence of PSA and alpha-1-antichymotrypsin in prostatic tissue sections," *Prostate Cancer P D* **2**, 140-147 (1999).
19. Y. Lu, G. L. Liu, J. Kim, Y. X. Mejia, and L. P. Lee, "Nanophotonic crescent moon structures with sharp edge for ultrasensitive biomolecular detection by local electromagnetic field enhancement effect," *Nano Lett* **5**, 119-124 (2005).

20. J. Malm, J. Hellman, P. Hogg, and H. Lilja, "Enzymatic action of prostate-specific antigen (PSA or hK3): substrate specificity and regulation by Zn(2+), a tight-binding inhibitor," *Prostate* **45**, 132-139 (2000).
21. C. V. Raman, "A change of wave-length in light scattering," *Nature* **121**, 619-619 (1928).
22. Y. Lu, G. L. Liu, and L. P. Lee, "High-density silver nanoparticle film with temperature-controllable interparticle spacing for a tunable surface enhanced Raman scattering substrate," *Nano Lett* **5**, 5-9 (2005).
23. A. J. Haes, L. Chang, W. L. Klein, and R. P. Van Duyne, "Detection of a biomarker for Alzheimer's disease from synthetic and clinical samples using a nanoscale optical biosensor," *J Am Chem Soc* **127**, 2264-2271 (2005).
24. J. B. Jackson, and N. J. Halas, "Surface-enhanced Raman scattering on tunable plasmonic nanoparticle substrates," *P Natl Acad Sci USA* **101**, 17930-17935 (2004).
25. S. Nie, and S. R. Emory, "Probing Single Molecules and Single Nanoparticles by Surface-Enhanced Raman Scattering," *Science* **275**, 1102-1106 (1997).
26. G. L. Liu, and L. P. Lee, "Nanowell surface enhanced Raman scattering arrays fabricated by soft-lithography for lable-free biomolecular detections in integrated microfluidics," *Appl. Phys. Lett.* **87**, 074101 (2005).
27. V.-D. Tuan, L. R. Allain, and D. L. Stokes, "Cancer gene detection using surface-enhanced Raman scattering (SERS)," J. Raman Spec. **33**, 511-516 (2002)
28. S. R. Denmeade et al, "Specific and efficient peptide substrates for assaying the proteolytic activity of prostate-specific antigen," *Cancer Res* **57**, 4924-4930 (1997).
29. G. L. Liu, Y. Lu, J. Kim, J. C. Doll, and L. P. Lee, "Magnetic Nanocrescents as Controllable Surface Enhanced Raman Scattering Nanoprobes for Biomolecular Imaging," *Adv. Mater.* **17**, 2683 (2005).

PART III SERS Detection of Peptide Phosphorylation

Src Protein-Tyrosin Kinase (PTK) is involved in many signaling pathway controlling cell activities such as proliferation, polarity, migration, and invasion. Src PTK is considered to have elevated levels and activities in various breast cancer cell lines; however the specific role of Src PTK in mammary cells is undefined. Src PTK is hypothesized to activate the downstream receptors such as EGFR-2 (HER-2) in the process of cancer invasion. Real-time imaging of the Src PTK activation and related EGFR-2 expression in living mammary cells upon various stimulations is essential for discovering the inducing mechanism and effective therapy for breast cancers, however effective fluorescence detection methods for in vivo phosphorylation reaction are absent to date. Here we demonstrate the dynamic molecular imaging of Src PTK phosphorylation in single breast cancer cell using intracellular surface enhanced Raman scattering (SERS) spectroscopy with submicron spatial resolution and 10-sec temporal resolution. After the Src activation is detected, the EGFR-2 level at the membrane of the same cell is monitored. Measured is not only the location of the Src phosphorylation events in the single cell, but also the accurate timing of the whole Src-mediated EGFR-2 pathway. The abundant spatiotemporal information in the dynamic imaging provides new physiological and pathological insights to the mechanism of breast cancers.

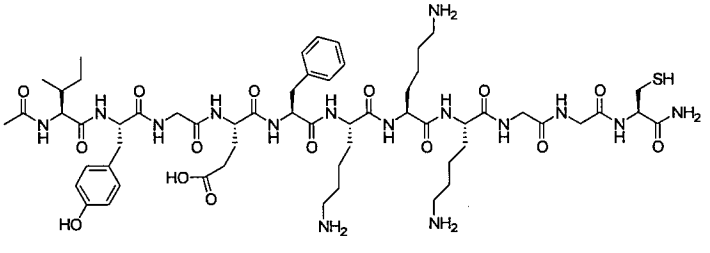

(a)

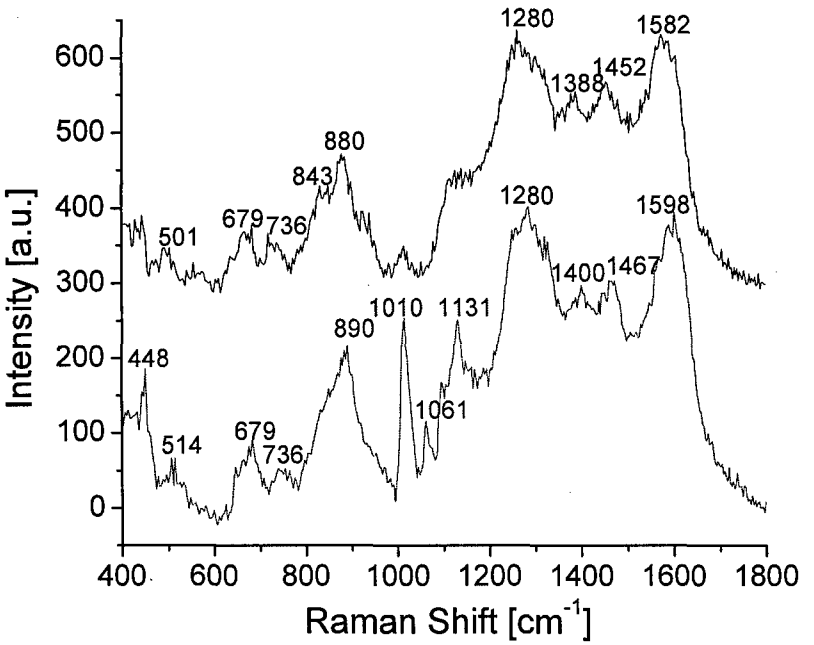

(b)

Fig. 1 (a) Chemical formula of p60c-Src peptide. (b) SERS spectra of p60c-Src peptide before (upper) and after (lower) the phosphorylation reactions with 100 nM tyrosine kinase.

Before the *in vivo* experiment, the nanocrescent particles modified with p60-Src peptides are tested with the activated protein tyrosine kinase (PTK) in ATP buffer. The ratio between the numbers of particles and peptides is 1:1000. The src-PTK concentration in the *in vitro* sample is around 100 nM. The phosphorylation site on the p60-Src peptides is the tyrosine residue. As shown in Fig. 1, some Raman peaks are identical before and after the phosphorylation reactions, while other peaks associated with tyrosine residues shifted after the reaction. The peaks, 501 cm^{-1}, 880 cm^{-1}, 1388 cm^{-1}, 1452 cm^{-1}, and 1582 cm^{-1} red shifted to 514 cm^{-1}, 890 cm^{-1}, 1400 cm^{-1}, 1467 cm^{-1} and 1598 cm^{-1} respectively. The intensity of peak 1010 cm^{-1} increases dramatically after the phosphorylation reactions. Two new peaks, 1061 cm^{-1} and 1131 cm^{-1}, rise after the reactions.

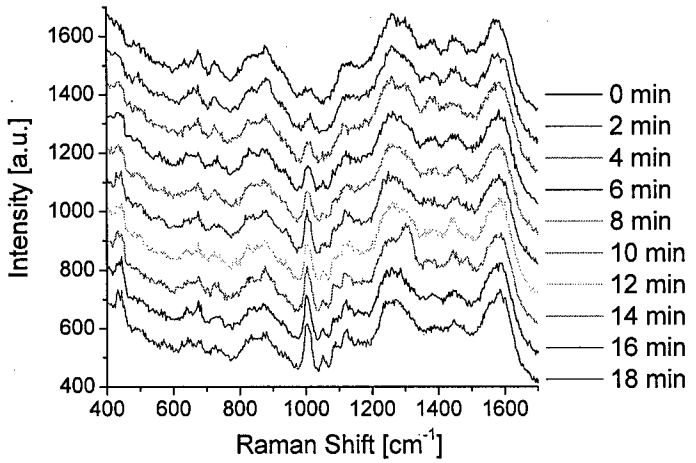

Fig. 2 Time-lapse SERS spectra in the phosphorylation reaction

The process of peptide phosphorylation can be probed by continuously measuring the SERS spectra. Figure 2 shows the SERS spectra of the peptides at different moments of the reactions. 100 nM p60c-Src peptides are added at 2 min time point and the spectra start to show apparent difference within 4 minutes. The binding of large numbers of Src-PTK with the peptides on particle surface will induce temporary violent change of the spectra as shown in Fig. 3. After the binding and phosphorylation are finished, the Src-PTK will detach from the peptide and the particle surface; therefore the spectra regain the original shape. Figure 4 shows the intensities of two characteristic peaks as the function of time.

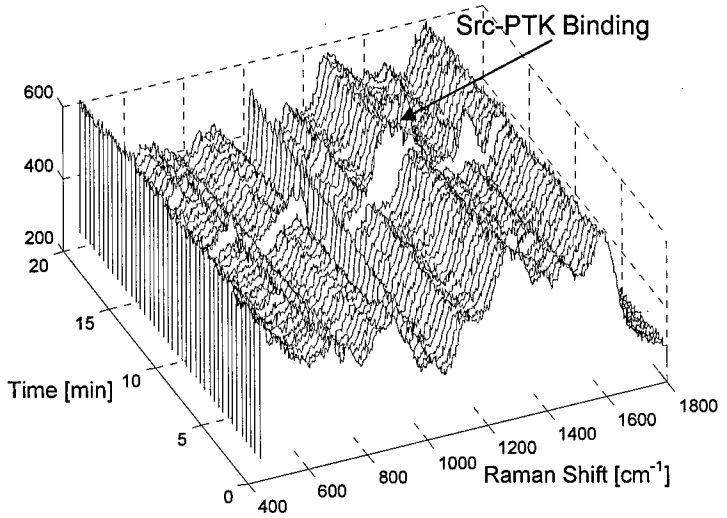

Fig. 3 Waterfall plot of time-lapse SERS spectra of Src peptides

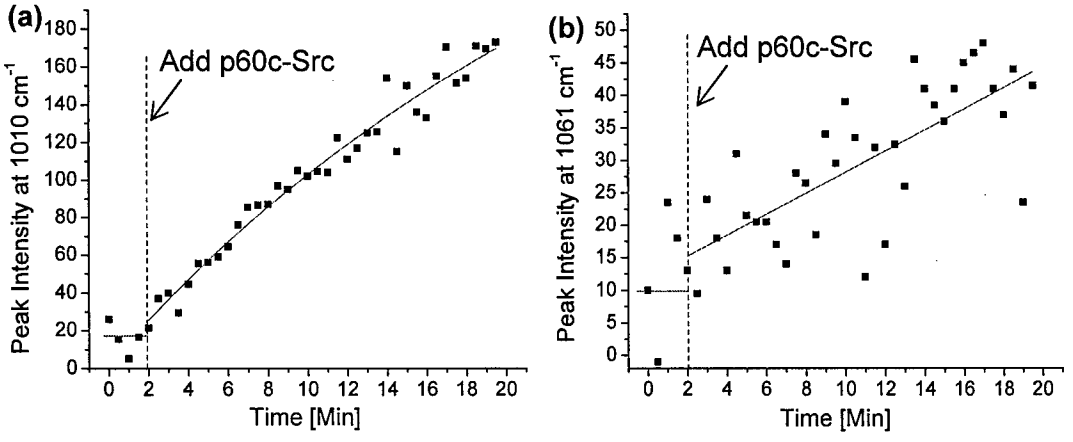

Fig. 4 **(a)** Intensity of peak 1010 cm^{-1} vs. time **(b)** Intensity of peak 1061 cm^{-1} vs time. The p60c-Src PTK is added at 2 min time point.

After the in vitro experiments, we incubate the peptide-conjugated nanocrescent particles with MCF-7 breast cancer cells. The nanocrescent particles can be internalized inside cells due to endocytosis. We then investigated the SERS spectrum of the nanocrescent particles residing in living cells. Figure 5 shows the phase contrast image of the cells and the SERS spectra acquired from the potential particle.

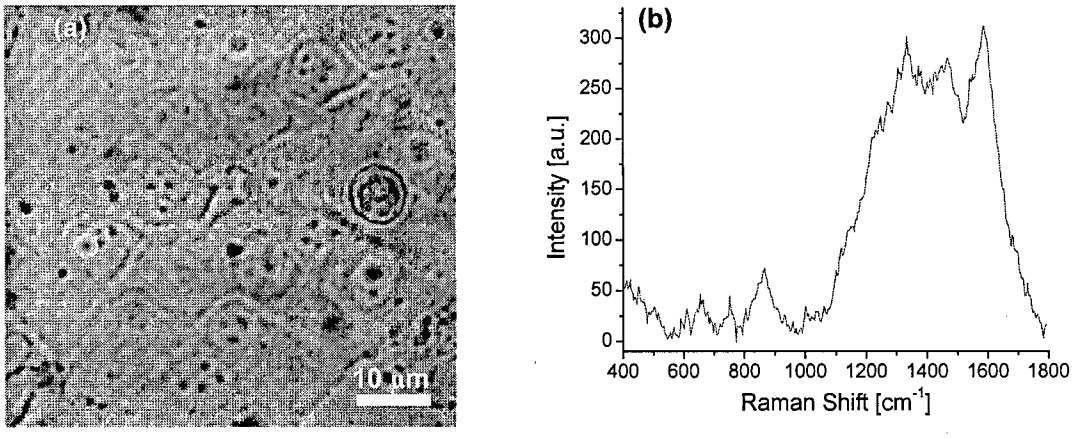

Fig. 5 (a) phase contrast image of the MCF-7 cells growing on a glass slide. The peptide-conjugated nanocrescent particles are incubated with cells. The red dot represents the laser excitation spot. (b) SERS spectra from the intracellular nanocrescent particle.